THE JOURNAL OF BIOLOGICAL CHEMISTRY VOL. 284, NO. 36, pp. 24257–24268, September 4, 2009

Role of Intramembrane Polar Residues in the YgfO Xanthine Permease

HIS-31 AND ASN-93 ARE CRUCIAL FOR AFFINITY AND SPECIFICITY, AND ASP-304 AND GLU-272 ARE IRREPLACEABLE[S]

Received for publication, June 6, 2009 Published, JBC Papers in Press, July 6, 2009, DOI 10.1074/jbc.M109.030734

Ekaterini Karena and Stathis Frillingos[1]

From the Laboratory of Biological Chemistry, University of Ioannina Medical School, 45110 Ioannina, Greece

Using the YgfO xanthine permease of *Escherichia coli* as a bacterial model for the study of the evolutionarily ubiquitous nucleobase-ascorbate transporter (NAT/NCS2) family, we performed a systematic Cys-scanning and site-directed mutagenesis of 14 putatively charged (Asp, Glu, His, Lys, or Arg) and 7 highly polar (Gln or Asn) residues that are predicted to lie in transmembrane helices (TMs). Of 21 single-Cys mutants engineered in the background of a functional YgfO devoid of Cys residues (C-less), only four are inactive or have marginal activity (H31C, N93C, E272C, D304C). The 4 residues are conserved throughout the family in TM1 (His-31), TM3 (Asn-93/Ser/Thr), TM8 (Glu-272), and putative TM9a (Asp-304/Asn/Glu). Extensive site-directed mutagenesis in wild-type background showed that H31N and H31Q have high activity and affinity for xanthine but H31Q recognizes novel purine bases and analogues, whereas H31C and H31L have impaired affinity for xanthine and analogues, and H31K or H31R impairs expression in the membrane. N93S and N93A are highly active but more promiscuous for recognition of analogues at the imidazole moiety of substrate, N93D has low activity, N93T has low affinity for xanthine or analogues, and N93Q or N93C is inactive. All mutants replacing Glu-272 or Asp-304, including E272D, E272Q, D304E, and D304N, are inactive, although expressed to high levels in the membrane. Finally, one of the 17 assayable single-Cys mutants, Q258C, was sensitive to inactivation by *N*-ethylmaleimide. The findings suggest that polar residues important for the function of YgfO cluster in TMs 1, 3, 8 and 9a.

The nucleobase-ascorbate transporter (NAT)[2] or nucleobase-cation symporter-2 (NCS2) family is an evolutionarily ubiquitous family of purine, pyrimidine, and L-ascorbate transporters, with members specific for cellular uptake of uracil, xanthine, or uric acid (microbial and plant genomes) or vitamin C (mammalian genomes) (1, 2). Despite their importance for the recognition and uptake of several frontline purine-related drugs, NAT/NCS2 members have not been studied systematically at the molecular level, and high resolution structures or mechanistic models are missing. More than 1000 sequence entries are known, but few have been functionally characterized to date. The best studied eukaryotic member is UapA, a high affinity uric acid/xanthine:H^+ symporter from the ascomycote *Aspergillus nidulans* (3–7). Studies with chimeric transporter constructs (3), site-directed mutagenesis, second-site suppressors, and kinetic inhibition analysis of ligand specificity have shown that a conserved NAT/NCS2 motif region between putative transmembrane helices 8 and 9 of UapA includes determinants of substrate recognition and selectivity, with at least one residue (Gln-408) implicated in binding with the imidazole moiety of purine (4), whereas a conserved QH motif at the middle of TM1 is important for activity and/or correct targeting to the plasma membrane (5), and an aromatic residue at the middle of TM12 (Phe-528) may act as a purine substrate selectivity filter (6). It has been proposed that TM1, TM12, and the NAT motif region interact functionally to determine affinity and specificity for uric acid (7).

Recently, we characterized the first purine-specific members of the NAT/NCS2 family from a Gram-negative bacterium, namely YgfO and YicE of *Escherichia coli* K-12 (8), as high affinity xanthine:H^+ symporters that cannot use uric acid, hypoxanthine, uracil, or other nucleobases as a substrate and cannot recognize analogues substituted at positions 7 or 8 of the imidazole ring. We launched a systematic series of Cys-scanning and site-directed mutagenesis studies of YgfO to elucidate structure-function relationships in a bacterial NAT (9, 10). In the course of these studies, we showed that the NAT motif sequence region of YgfO includes the essential determinants Gln-324, irreplaceable for high affinity binding and uptake; Asn-325, irreplaceable for active transport; and an α-helical stripe of residues (Thr-332, Gly-333, Ser-336, Val-339), highly sensitive to site-directed alkylation and important for ligand selectivity[3] (9). In addition, we provided evidence that Asn-430 of TM12 is close to the purine binding site and Ile-432 optimizes binding indirectly (10). These studies also show that the bacterial (9, 10) and fungal (4, 6) NAT determinants are strikingly similar, implying that few of the residues conserved within the members of NAT family may be invariably critical for function.

In this report, we have studied the highly polar (Gln or Asn) and putatively charged (Asp, Glu, His, Lys, or Arg) residues of

[S] The on-line version of this article (available at http://www.jbc.org) contains supplemental Tables S1–S3 and references therein.

[1] To whom correspondence should be addressed. E-mail: efriligo@cc.uoi.gr.

[2] The abbreviations used are: NAT, nucleobase-ascorbate transporter; TM, transmembrane helix; IPTG, isopropyl 1-thio-β,D-galactopyranoside; HRP, horseradish peroxidase; BAD, biotin acceptor domain; Cys-less (C-less), permease devoid of native Cys residues; NEM, *N*-ethylmaleimide; SCAM, substituted-cysteine accessibility method; SVCT, sodium-dependent vitamin C transporter.

[3] E. Georgopoulou and S. Frillingos, manuscript in preparation.

YgfO permease that are predicted to lie in transmembrane helices. Such residues are expected to face other hydrophilic parts of the protein and/or the solvent-accessible environment of the binding pocket and often play crucial roles in substrate binding and the mechanism of energy coupling in active transport (11–14). Employing systematic site-directed mutagenesis of a set of 14 putatively charged and 7 highly polar residues predicted to lie in TMs (Fig. 1) and combining evidence from transport, immunoblotting, sulfhydryl alkylation, and ligand inhibition assays of a set of 60 site-directed mutants, we have identified four new important determinants in the YgfO mechanism: His-31 and Asn-93, which are crucial for affinity and/or specificity of binding purine analogues; and Glu-272 and Asp-304, which are irreplaceable for active xanthine transport. The results are discussed in conjunction with our previous findings on the role of TM12 and the NAT motif region and with respect to comparison with the major fungal homolog (UapA).

EXPERIMENTAL PROCEDURES

Materials—[8-^{3}H]Xanthine (27.6 Ci mmol^{-1}) and [8-^{14}C]uric acid (51.5 mCi mmol^{-1}) were purchased from Moravek Biochemicals. Non-radioactive nucleobases and analogues were from Sigma. Oligodeoxynucleotides were synthesized from BioSpring GmbH. High fidelity *Taq* polymerase (Phusion High Fidelity PCR System) was from Finnzymes. Restriction endonucleases used were from Takara. Horseradish peroxidase (HRP)-conjugated avidin was from Amersham Biosciences. HRP-conjugated penta-His antibody was from Qiagen. All other materials were reagent grade and were obtained from commercial sources.

Bacterial Strains and Plasmids—*E. coli* K-12 was transformed according to Inoue *et al*. (15). TOP10F′ (Invitrogen) was used for the initial propagation of recombinant plasmids. T184 (16) harboring pT7-5/*ygfO* (8) with given replacements was used for IPTG-inducible expression from the *lacZ* promoter/operator.

DNA Manipulations—Construction of expression plasmids and BAD (biotin acceptor domain)-tagged versions of YgfO containing a C-terminal tail with the BAD of *Klebsiella pneumoniae* oxaloacetate decarboxylase and the C-terminal 12 peptides of *E. coli* LacY has been described (8). Construction of the His_{10}-tagged versions has also been described (9). For construction of Cys-less YgfO, the five native Cys codons were replaced simultaneously with Ser codons using two-stage (multiple overlap/extension) PCR on the template of wild-type YgfO tagged at the C terminus with the BAD tag and transferred to the His_{10}-tagged background by BamHI-HpaI restriction fragment replacement (10). For construction of mutants, two-stage PCR was performed on the template of Cys-less or wild-type YgfO tagged at the C terminus with either BAD or His_{10} as indicated. The entire coding sequence of all engineered constructs was verified by double-stranded DNA sequencing in an automated DNA sequencer (MWG-Biotech).

Growth of Bacteria—*E. coli* T184 harboring given plasmids was grown aerobically at 37 °C in Luria-Bertani medium containing streptomycin (0.01 mg/ml) and ampicillin (0.1 mg/ml). Fully grown cultures were diluted 10-fold, allowed to grow to mid-logarithmic phase, induced with IPTG (0.5 mM) for an additional 2 h at 37 °C, harvested, and washed with the appropriate buffers.

Transport Assays and Kinetic Analysis—*E. coli* T184 were assayed for active transport of [^{3}H]xanthine (1 μM) by rapid filtration, at both 25 and 37 °C, as described (8). For kinetic uptake measurements, initial rates were assayed at 5–20 s in the concentration range of 0.1 to 100 μM [^{3}H]xanthine. Selected mutants were also assayed for transport of [^{14}C]uric acid (0.04–2 mM) using the paralog YgfU (Fig. 2) as a positive control.[4] For assaying the effect of *N*-ethylmaleimide (NEM) on xanthine uptake activity, T184 cells were preincubated with NEM at the indicated conditions, reactions were stopped by the addition of a 20-fold excess of dithiothreitol, excess reagents, and ligands were removed by centrifugation. Transport assays were performed in the presence of phenazine methosulfate (0.2 mM) and potassium ascorbate (20 mM) (10). For ligand competition experiments, uptake of [^{3}H]xanthine (1 μM) was assayed in the absence or presence of unlabeled analogues (1 mM) (8). Competitive inhibition has been revealed with certain analogues (1-methyl-, 2-thio-, and 8-methylxanthine) by assaying their effect on K_m and V_{max} for wild type and selected mutants, showing that V_{max} remains unaltered (9, 10).

Immunoblot Analysis—Membrane fractions of *E. coli* T184 harboring the given plasmids were prepared and subjected to SDS-PAGE (12%) as described (8). Proteins were electroblotted to polyvinylidene difluoride membranes (Immobilon PVDF; Pall Corp.). YgfO-BAD was probed with avidin-HRP and YgfO-His_{10} with penta-His antibody-HRP. Signals were developed with enhanced chemiluminescence (ECL).

In Silico Analysis—Comparative sequence analysis of NAT/NCS2 homologs was based on a BLAST-p search and ClustalW alignment, and the most recent genome annotations were used to retrieve sequence data. Based on the functional (8) and phylogenetic data,[5] the YgfO permease recently has been renamed XanQ (EcoGene data base of *E. coli* sequence and function). Initial analysis of transmembrane topology was performed using the program TMHMM (17).

RESULTS

Delineation of Polar Residues That Fall in TMs—Based on prediction algorithms, experimental evidence on the cytoplasmic orientation of the C terminus (8, 17), and SCAM analysis data,[6] we deduced a model for the topological organization of YgfO permease in which 26 highly polar or putatively charged residues fall in the TMs (Fig. 1). These residues are: His-22, Gln-23, Thr-30, His-31, Glu-55, Gln-90, Asn-93, Lys-164, Asn-184, Glu-186, His-187, Asp-232, Lys-249, His-257, Gln-258, Glu-272, Asp-304, Gln-330, Arg-337, Arg-341, Arg-385, Asn-390, Asp-413, Glu-429, Asn-430, Asn-443. Of them, Asp-304 falls in a putatively transmembrane α-helical segment of ambiguous topology, preceding the NAT signature motif sequence (9), which we designate TM9a (Fig. 1), and Thr-30 is included in the group of the highly polar (Gln/Asn) resi-

[4] K. Papakostas and S. Frillingos, manuscript in preparation.
[5] Kenn Rudd, personal communication.
[6] G. Mermelekas and S. Frillingos, manuscript in preparation.

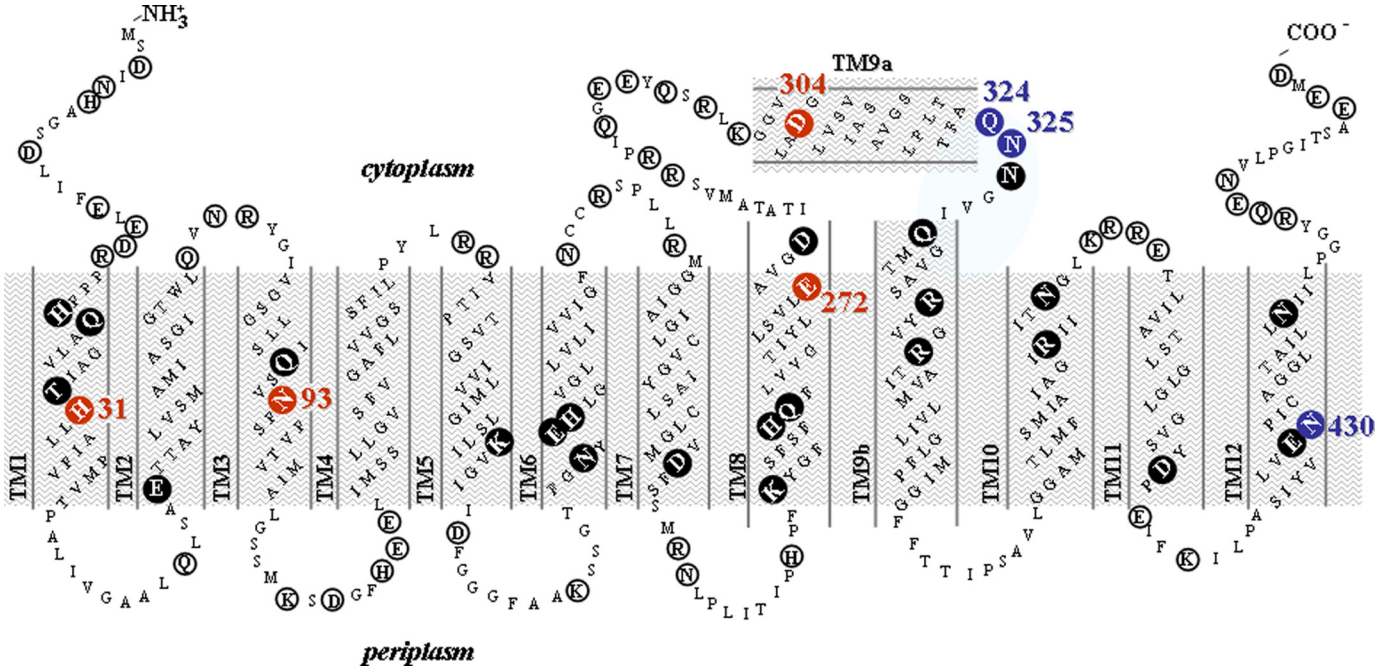

FIGURE 1. **Proposed topology of YgfO highlighting the polar/charged residues.** This model is based on the program TMHMM, evidence that the C terminus is cytoplasmic (10, 25), and our unpublished evidence[6] on the accessibility of loops to hydrophilic reagents from SCAM analysis. Putatively charged (K/R/H/D/E) or highly polar (Q/H) residues are *enlarged* and *circled*. Residues that fall in transmembrane helices (TMs) or in the NAT motif sequence (residues 323–333), as well as residue Asp-276 (which is discussed under "Discussion") are shown with a *dark background*. Residues delineated as important to our studies are *numbered* and shown in *red* (this study) or *blue* (previous studies). The ambiguous topology segment 299–323 upstream of the NAT motif is designated as TM9a, and the transmembrane segment 330–357 that follows is designated as TM9b. SCAM analysis[6] of the NAT motif shows that residues 323–333 are accessible to solvent from the outside (*light blue-gray* area), indicating that this region is topologically dynamic and might constitute a flexible, substrate-accessible (7, 9) reentry loop.

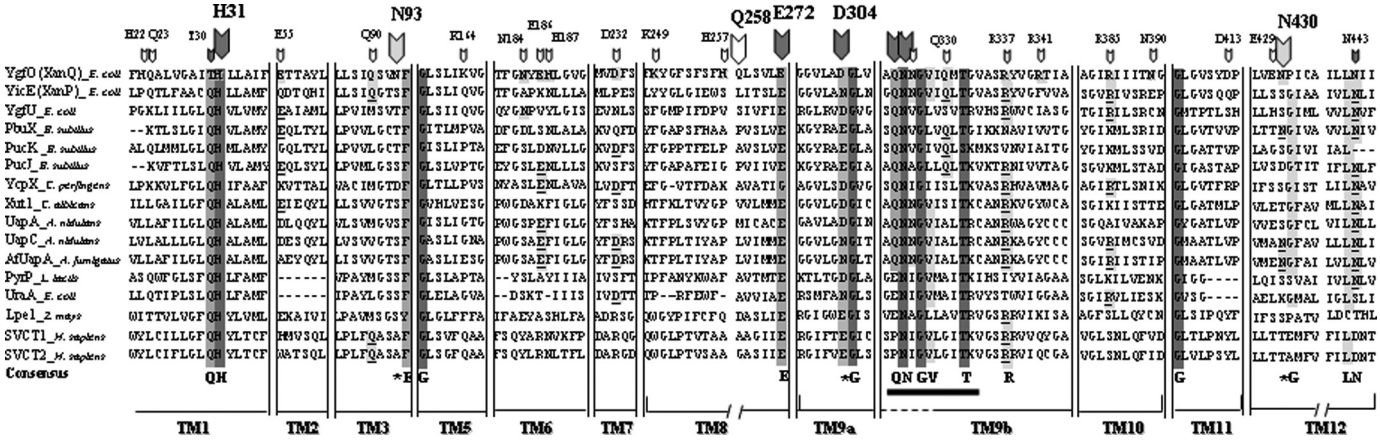

FIGURE 2. **Sequence alignment of segments containing putative intramembrane polar residues of YgfO.** Shown is a consensus of the 16 characterized NAT/NCS2 transporters (with GenBank™ accession numbers in parentheses): *E. coli* YgfO (XanQ) (P67444), YicE (XanP) (P0AGM9), YgfU (Q46821),[6] and UraA (P0AGM7); *Bacillus subtilis* PbuX (P42086), PucK (O32140), and PucJ (O32139); *Clostridium perfringens* YcpX (BAB80103); *Lactococcus lactis* PyrP (AAK05701); *A. nidulans* UapA (Q07307) and UapC (P487777); *Aspergillus fumigatus* AfUapA (XP748919); *Candida albicans* Xut1 (AAX2221); *Zea mays* Lpe1 (AAB17501); *Homo sapiens* SVCT1 (SLC23A1) (AAH50261) and SVCT2 (SLC23A2) (Q9UGH3). The full-length sequences were aligned using ClustalW and part of this alignment including the residues of interest is presented. *Cuneiform symbols* denote the positions of a highly polar/charged residue in YgfO. *Larger cuneiforms* indicate residues delineated as important from work presented herein or previous analyses (9, 10). *Filled cuneiforms* denote highly conserved polar residues. Residues similar to the consensus are *shaded*, and highly conserved residue positions are indicated with *continuous vertical shading*. An *asterisk* in the consensus sequence denotes positions conserving a polar character of the side chain but not the side chain *per se*. The NAT signature motif sequence (9) is indicated by a *bold horizontal bar*.

dues (18), as all other NAT transporters conserve a Gln at the corresponding position (Fig. 2). Interestingly, the bulk of the 26 residues falls in only six TMs of YgfO (TMs 1, 3, 6, 8, 9a, 9b, and 12); residues falling in TM1 (His-31), TM8 (Glu-272), TM9a (Asp-304), and TM12 (Asn-443) are highly conserved in the NAT family, whereas Asn-93 (TM3) and Asn-430 (TM12) are not conserved *per se* but are conserved with respect to the polar character of the side chain (Asn, Ser, or Thr, at the corresponding positions) (Fig. 2). Of the cohort of 26 residues, five (Gln-330, Arg-337, Glu-429, Asn-430, and Asn-443) have already been studied by us in the context of previous Cys-scanning analyses (9, 10). Thus, we selected the remaining 21 residues (Fig. 1) for a systematic site-directed mutagenesis study.

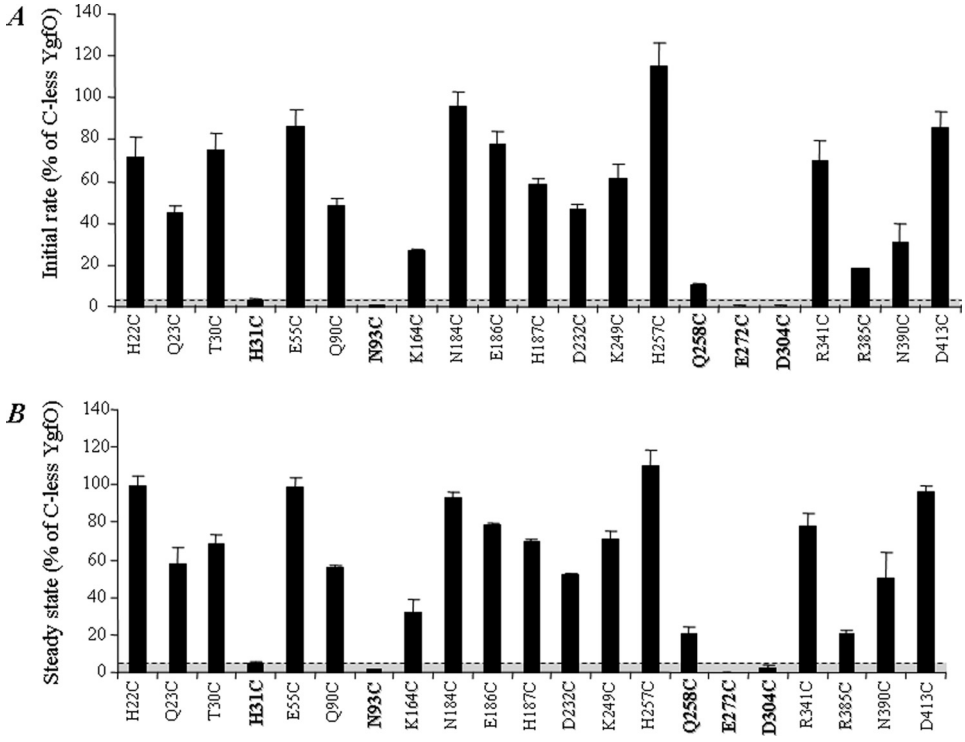

FIGURE 3. **Active xanthine transport activities of single-Cys mutants.** *E. coli* T184 harboring pT7-5/*ygfO*(C-less-BAD) with the given mutations was grown aerobically at 37 °C in complete medium to mid-logarithmic phase, induced with IPTG (0.5 mM) for 2 h, normalized to 0.7 mg of protein/ml of cell suspension, and assayed for transport of [^{3}H]xanthine (1 μM) at 25 °C. *A*, initial rates of uptake measured at 5–20 s. Control values obtained from T184 harboring pT7-5 alone (0.015 nmol mg^{-1} min^{-1} on average) were subtracted from the sample measurements in all cases. Results are expressed as a percentage of the rate of Cys-less YgfO (1.8 nmol mg^{-1} min^{-1} on average) with standard deviations from three independent determinations. *B*, steady state levels of xanthine accumulation (reached at 1–10 min for most mutants). Control values obtained from T184 harboring pT7-5 alone (0.01 nmol mg^{-1} on average) were subtracted from the sample measurements in all cases. Results are expressed as a percentage of the level of Cys-less YgfO (0.8 nmol mg^{-1} on average) with standard deviations from three independent determinations.

Active Xanthine Transport of Single-Cys Mutants—Using a functional YgfO devoid of Cys residues (C-less), we replaced each of the 21 putative intramembrane polar amino acid residues (Fig. 1) individually with Cys. After verification of the sequence, each single-Cys mutant was transformed into *E. coli* T184 and assayed for its ability to catalyze active xanthine transport. As shown in Fig. 3*A*, of the 21 single-Cys mutants, 13 transport xanthine at rates between 45 and 100% or more of C-less permease, N390C transports at a rate of 35% of C-less, and an additional three mutants (K164C, Q258C. and R385C) transport at rates that are between 15 and 25% of C-less. One mutant (H31C) displays a very low but detectable uptake rate (5% of C-less). Finally, mutants N93C, E272C and D304C display rates that approximate cells transformed with vector containing no *ygfO* insert. Steady state levels of xanthine accumulation also show the same general picture (Fig. 3*B*). Of the 21 single-Cys mutants, 14 accumulate xanthine to more than 55% of the steady state observed with C-less YgfO, and an additional 3 mutants (K164C, Q258C, and R385C) exhibit levels of 20–35%. Of the remaining 4 mutants, H31C accumulates marginally (5% of C-less), whereas N93C, E272C, and D304C are inactive.

Expression in the Membrane—Immunoblot analysis of BAD-tagged single-Cys permeases shows that most mutants, including the marginally active H31C and the inactive E272C and D304C, are expressed to high levels comparable with those of C-less YgfO or higher (Fig. 4). The compromised expression (~25–45% of C-less) displayed by mutants K164C, D232C, Q258C, and R385C reflects their relatively low transport rates (15–45% of C-less) (Fig. 3). The inactive N93C also displays low but significant expression in the membrane (25% of C-less).

Expression and Transport Analysis of Mutants in Wild-type Background—From the Cys-scanning transport analysis described above, eight positions of inactive, low activity, and/or low expression mutants were delineated. We analyzed these positions further by (*a*) transferring single-Cys mutations to the wild-type YgfO background and/or (*b*) engineering a most conservative site-directed replacement mutant to introduce an amino acid other than Cys. Thus, we constructed and assayed mutants (*a*) H31C(wt), N93C(wt), K164C(wt), D232C(wt), Q258C(wt), E272C(wt), D304C(wt), and R385C(wt) and (*b*) N93Q(wt), K164R(wt), D232E(wt), Q258N(wt), E272D(wt), D304E(wt), and R385K(wt) (Fig. 5). Of the Cys-replacement mutants, K164C(wt) is highly active (80% of wild type), H31C(wt), D232C(wt), Q258C(wt), and R385C(wt) display low but significant activity (25–40% of wild type), N93C(wt) transports marginally (5% of wild-type), while E272C(wt) and D304C(wt) display negligible activity (Fig. 5*A*). Of the second set of mutants, K164R(wt) displays higher activity than wild type (160%), D232E(wt), Q258N(wt), and R385K(wt) are highly active (50–90% of wild type), E272D(wt) and D304E(wt) display very low rates (5 and 2%, respectively) and levels of accumulation (30 and 10%, respectively), and N93Q(wt) is inactive (Fig. 5*B*). All mutants of the two sets are expressed in the *E. coli* membrane to high levels comparable with those of the wild type (Fig. 5).

Transport Analysis of Site-directed Mutants at Positions His-31, Asn-93, Glu-272, and Asp-304—The conserved (Fig. 2) positions His-31, Asn-93, Glu-272, and Asp-304, where mutants with negligible or strikingly low activity had been detected (Figs. 3 and 5), were further subjected to extensive site-directed mutagenesis in the wild-type YgfO background. Site-directed mutants were analyzed initially for expression, active xanthine transport (Figs. 6–8), and kinetics of xanthine uptake (Table 1).

Replacements of Glu-272 and Asp-304—Our data show that replacement of Glu-272 with Gln or Cys yields negligible activity, whereas replacement with Asp results in a mutant with marginally detectable xanthine uptake rate and a very low level of accumulation reached after 10 min (Fig. 6, *B* and *C*). Replacement of Asp-

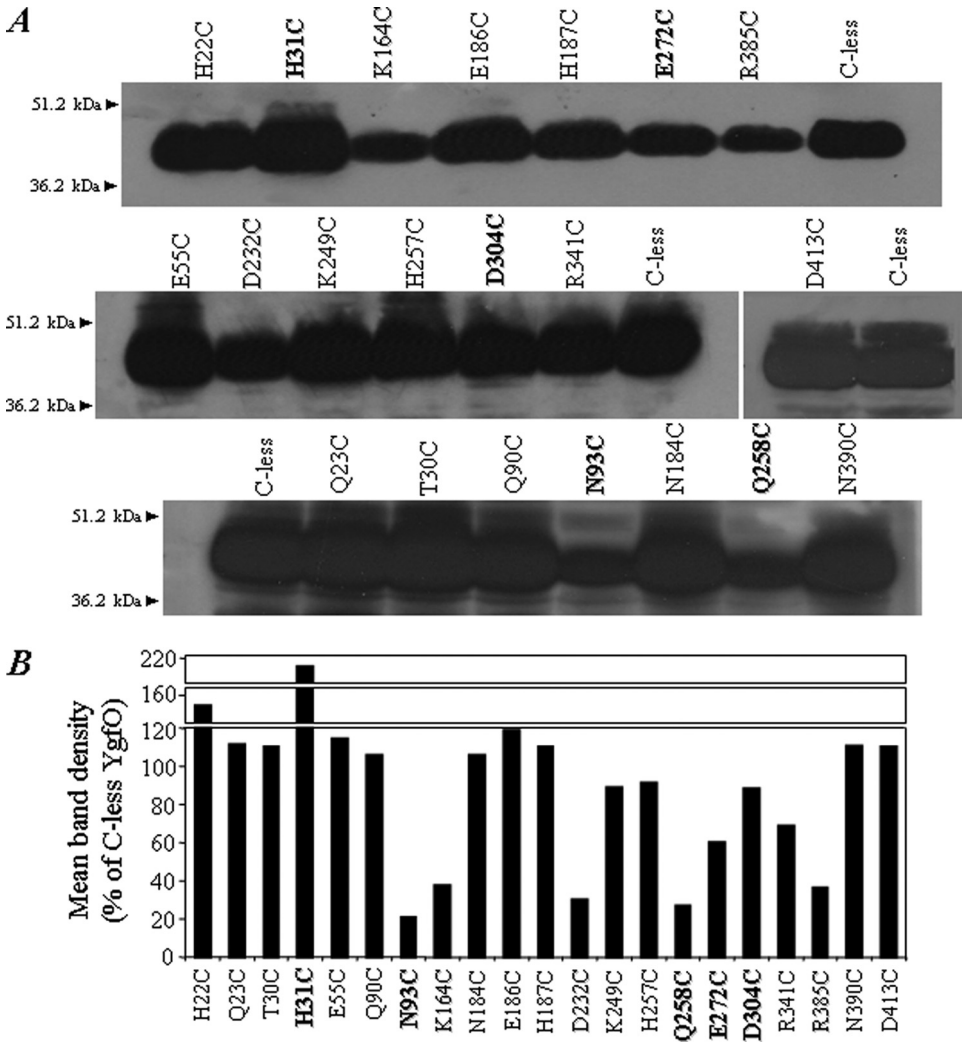

FIGURE 4. **Immunoblot analysis of single-Cys mutants.** Membranes were prepared from IPTG-induced cultures of *E. coli* T184 harboring pT7-5/*ygfO*(C-less-BAD) with given mutations. Samples containing ~100 μg of membrane protein were subjected to SDS-PAGE (12%) and immunoblotting using HRP-conjugated avidin. *A*, representative blots of single-Cys mutants and Cys-less YgfO. Membranes prepared from cells harboring pT7-5 alone exhibited no immunoreactive material. Prestained molecular weight standards (Bio-Rad, low range) are shown on the *left*. *B*, quantitative estimation of the expression level of each mutant as a percentage of Cys-less expression derived from the relative density of the corresponding band. Results shown are the means of four determinations from two independent experiments (S.D < 15%).

304 with Asn, Cys, or Glu also results in marginally active or inactive mutants. Kinetic analysis shows that mutants replacing Glu-272 or Asp-304 display very low or negligible rates of xanthine uptake at any of the concentrations tested, in the range 0.1 to 100 μM (Table 1). No xanthine uptake activity was detected for any of these mutants at pH ranging from 4.0 to 10.0 at either 25 or 37 °C, and no uptake of uric acid (0.04–2 mM) could be detected either (data not shown). Although inactive, these mutants are expressed in the membrane to wild-type levels (Fig. 6*A*). In addition, no activity of the inactive single-Cys mutants E272C and D304C (Fig. 3) was rescued by incubation with the negatively charged (2-sulfonatoethyl)methanethiosulfonate (19), and no uptake activity could be detected with double-Cys replacement mutants (20) E272C/H31C, D304C/H31C, E272C/R385C, and D304C/R385C or double replacement mutants harboring a conservative change of Glu-272 or Asp-304, including E272D/N430C, D304E/N430C, E272Q/N430C, D304N/N430C, E272D/N325C, D304E/N325C, E272Q/N325C, and D304N/N325C. All of these inactive mutants are expressed in the membrane to high levels (Fig. 6 and data not shown).

Replacements of His-31—Site-directed replacement of His-31 with a putatively positively charged residue, Arg or Lys, results in negligible activity, corroborated by negligible or marginally detectable expression in the membrane (Fig. 7). Replacement of His-31 with Leu or Cys results in intermediate activity (xanthine uptake rates and levels of 40–50% relative to wild type) and slightly compromised but high expression in the membrane (Fig. 7). Replacement of His-31 with Asn results in approximately wild-type levels of expression and xanthine uptake activity, and replacement with Gln results in 1.2–1.5-fold higher expression and xanthine uptake activity than wild type (Fig. 7). Kinetic transport analysis shows that mutants with Asn or Gln at position 31 display a K_m approximating wild type and a higher V_{max}, whereas mutants with Cys or Leu display high V_{max} but very low affinity, with a 10- or 5-fold increased K_m, respectively (Table 1).

Replacements of Asn-93—Although replacement of Asn-93 with Gln leads to inactivation of YgfO and replacement with Cys results in strikingly low activity (Fig. 5), replacement of Asn-93 with Asp or Thr yields low but significant xanthine uptake (10–15% of wild type), replacement with Ala yields high activity (60–70% of wild type), and replacement with Ser yields activity higher than wild type (1.8-fold higher rate and 1.2-fold higher level of accumulation) (Fig. 8, *lower panel*). There are no significant differences in the expression levels of these mutants in the membrane (Fig. 8, *upper panel*). Kinetic transport analysis reveals that mutants with Ser, Ala, or Asp at position 93 display higher affinity than wild type (2-fold decreased K_m) with higher, equivalent, or very low V_{max}, respectively, whereas mutant N93T displays lower affinity (2-fold increased K_m) and wild-type V_{max} (Table 1).

Ligand Recognition Profiles of Site-directed Mutants at Positions His-31 and Asn-93—To understand whether His-31 or Asn-93 contributes to the substrate and ligand recognition profile of YgfO, we assayed the active His-31 and Asn-93 mutants for inhibition of [^{3}H]xanthine uptake in the presence or absence of a series of purines and purine analogues (Table 2). Of

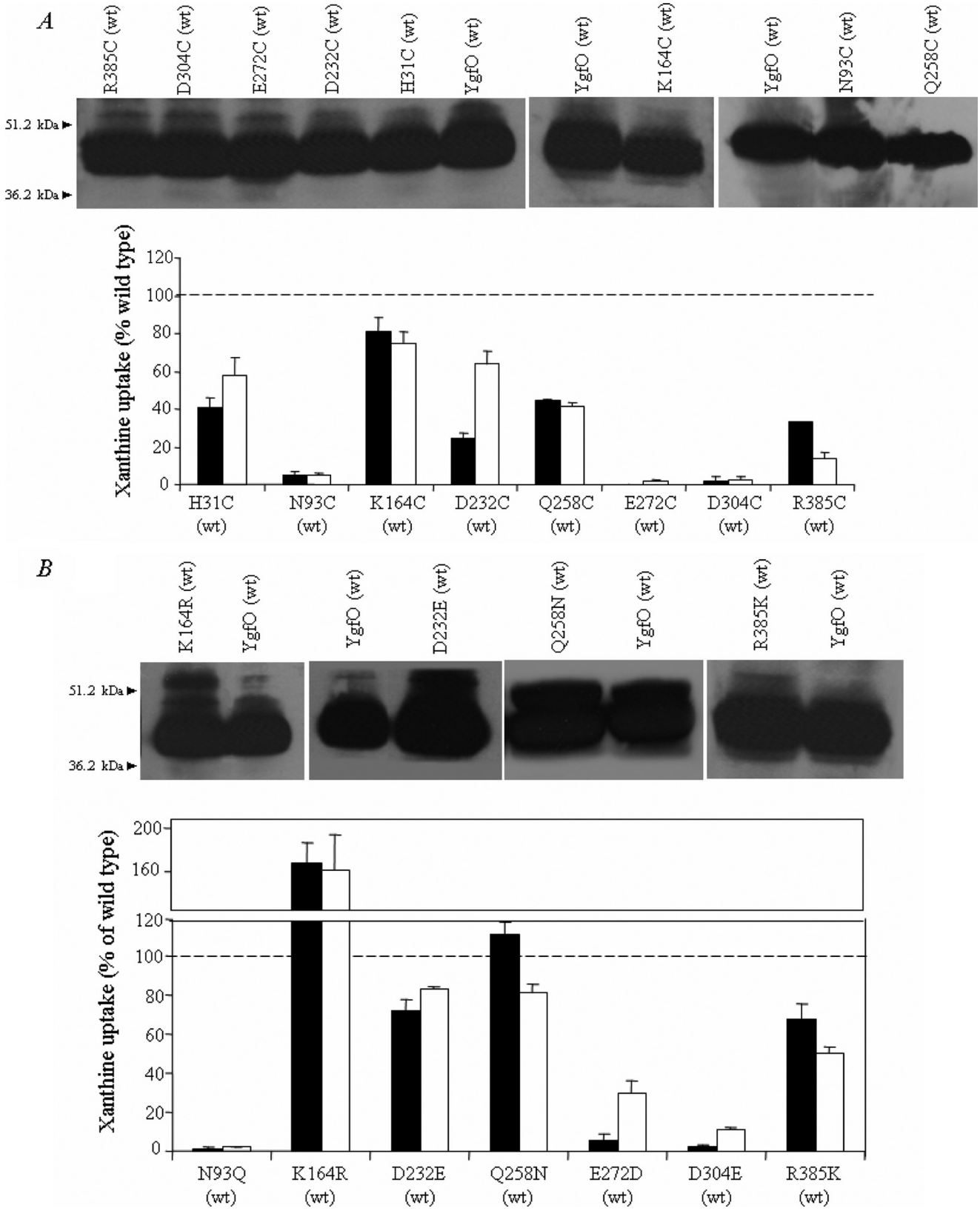

FIGURE 5. **Expression and xanthine uptake activities of Cys-replacement (*A*) and most conservative replacement mutants (*B*) in the wild-type permease background.** *E. coli* T184 harboring pT7-5/*ygfO*(wild-type-BAD) with given mutations were grown, induced, and subjected to immunoblot analysis of membrane fractions or assayed for transport of [^{3}H]xanthine (1 μM, 25 °C) exactly as described in the legends for Figs. 3 and 4. *Open* and *closed histogram bars* represent initial rate and steady state values, respectively, with standard deviations shown from three independent experiments.

TABLE 1

K_m and V_{max} values of YgfO mutants for xanthine uptake

E. coli T184 expressing the corresponding constructs were assayed for initial rates of xanthine uptake at 5–20 s in the concentration range of 0.1 to 100 μM. Negative control values obtained from T184 harboring vector pT7-5 alone were subtracted from the sample measurements in all cases. Kinetic parameters were determined from nonlinear regression fitting to the Michaelis-Menten equation using Prism4. Values represent the means of three independent determinations ± S.D. are shown. All mutants as well as the wild-type YgfO version used in these experiments contained a C-terminal BAD. ND, assays were performed, but kinetic values were not determined because of very low uptake rates (≤0.06 nmol mg^{-1} min^{-1}).

Permease	K_m	V_{max}	V_{max}/K_m
	μM	*nmol min^{-1} mg^{-1} protein*	μl min^{-1} mg^{-1}
YgfO(wt)	4.6 ± 0.3	6.4 ± 0.5	1391
YgfO (C-less)	5.5 ± 0.5	10.2 ± 0.9	1858
A			
H31C(wt)	47.4 ± 6.4	33.9 ± 2.7	715
H31L(wt)	26.1 ± 2.0	23.9 ± 0.8	919
H31N(wt)	2.7 ± 0.5	16.2 ± 0.8	5945
H31Q(wt)	3.4 ± 0.5	12.1 ± 0.5	3558
B			
N93A(wt)	2.4 ± 0.7	5.0 ± 0.4	2083
N93S(wt)	2.1 ± 0.9	16.7 ± 1.8	7952
N93T(wt)	11.6 ± 2.9	5.0 ± 0.4	431
N93D(wt)	2.3 ± 0.3	0.5 ± 0.1	217
N93C(wt)	ND	ND	
N93Q(wt)	ND	ND	
C			
E272D(wt)	ND	ND	
E272Q(wt)	ND	ND	
D304E(wt)		ND	ND
D304N(wt)	ND	ND	
D			
Q258N(wt)	2.7 ± 1.5	4.8 ± 0.7	1778
Q258H(wt)	2.5 ± 1.1	4.7 ± 0.8	1880

the His-31 mutants, H31C(wt) and H31L(wt) display an impaired ability for recognition of any of the analogues tested, consistent with their very low affinity for xanthine as revealed from the kinetics experiments (Tables 1 and 2); H31N(wt) shows a nearly wild-type profile but with a modest ability to recognize 8-methylxanthine and uric acid; finally, H31Q(wt) recognizes a broader range of purines and purine analogues than wild type, including uric acid, guanine, uracil, 7-methylxanthine, and 8-methylxanthine (Table 2). Of the Asn-93 mutants, N93A(wt) and N93S(wt) recognize uric acid, 7-methylxanthine, and, most strikingly, 8-methylxanthine, which are not recognized by wild type. The same trend is apparent for N93D(wt), whereas N93T(wt) displays a compromised ability to recognize all analogues, most notably 1-methylxanthine and 6-methylxanthine (Table 2). Mutants shown to recognize uric acid in the transport inhibition experiments were also assayed for active transport of [^{14}C]uric acid at concentrations of 0.04 to 2 mM. H31N(wt) and H31Q(wt) displayed no capacity for uric acid uptake, and N93A(wt) and N93S(wt) displayed low but clearly detectable uric acid uptake at 2 mM (data not shown).

Effect of N-Ethylmaleimide on Transport Activity—The effect of NEM, a membrane-permeable sulfhydryl reagent, on the initial rate of xanthine transport for each single-Cys mutant is presented in Fig. 9. Of 17 active single-Cys mutants (Fig. 3) only Q258C is inhibited significantly (by ~50%) after incubation with 2 mM NEM (Fig. 9). No protection or enhancement of this

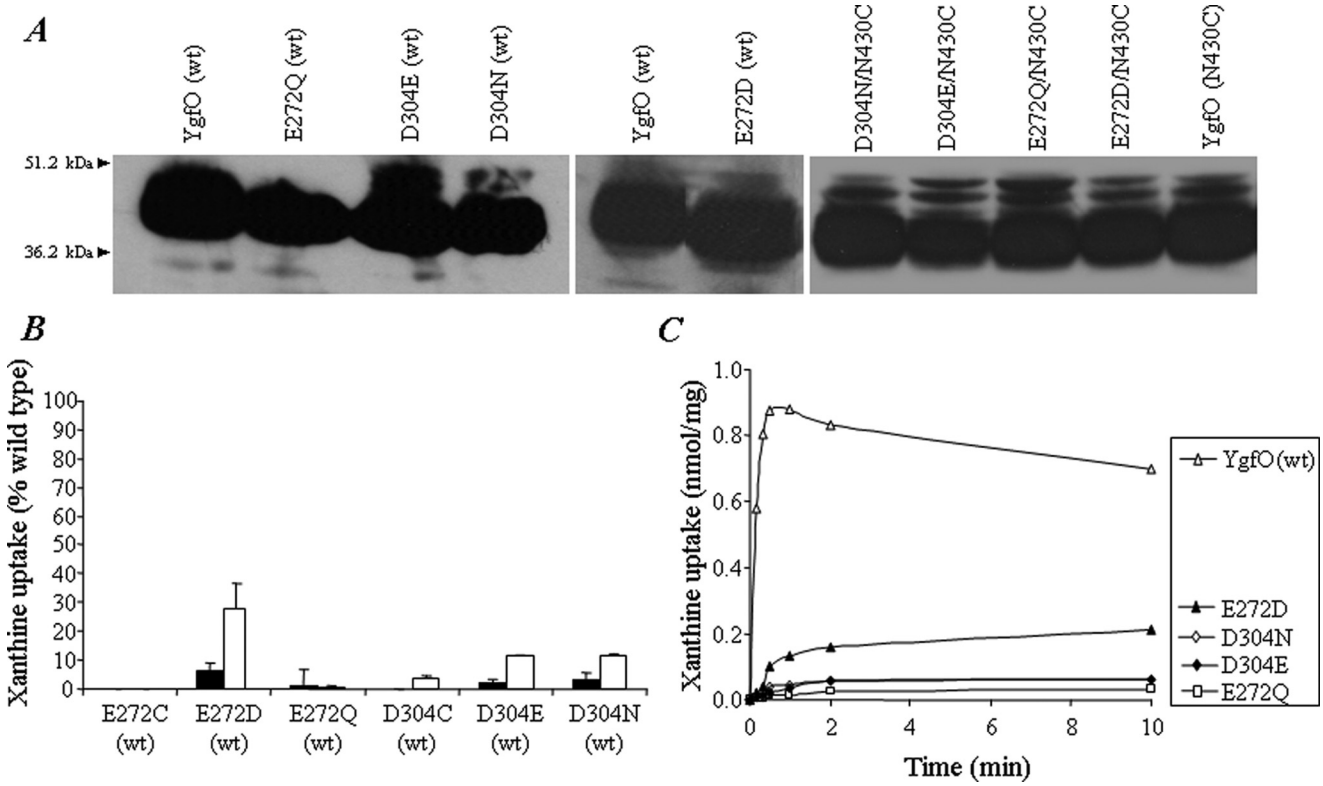

FIGURE 6. **Expression and xanthine uptake activities of site-directed mutants at positions 272 and 304.** *E. coli* T184 harboring pT7-5/*ygfO*(wild-type-BAD) or pT7-5/*ygfO*(C-less-His$_{10}$) with given mutations were grown, induced, and subjected to immunoblot analysis of membrane fractions (*A*) or assayed for transport of [^{3}H]xanthine (1 μM, 25 °C) (*B* and *C*) exactly as described in the legends to Figs. 3 and 4. *Open* and *closed histogram bars* (in *B*) represent the initial rate and steady state values, respectively, with standard deviations shown from three independent experiments. *C*, representative time courses of xanthine uptake by mutants E272D(wt), D304E(wt), D304N(wt), and E272Q(wt) in comparison with wild-type YgfO. Although not shown, values for E272Q(wt) were indistinguishable from negative controls (cells harboring pT7-5 alone) or double replacement mutants with a change at Glu-272 or Asp-304 (see under "Results").

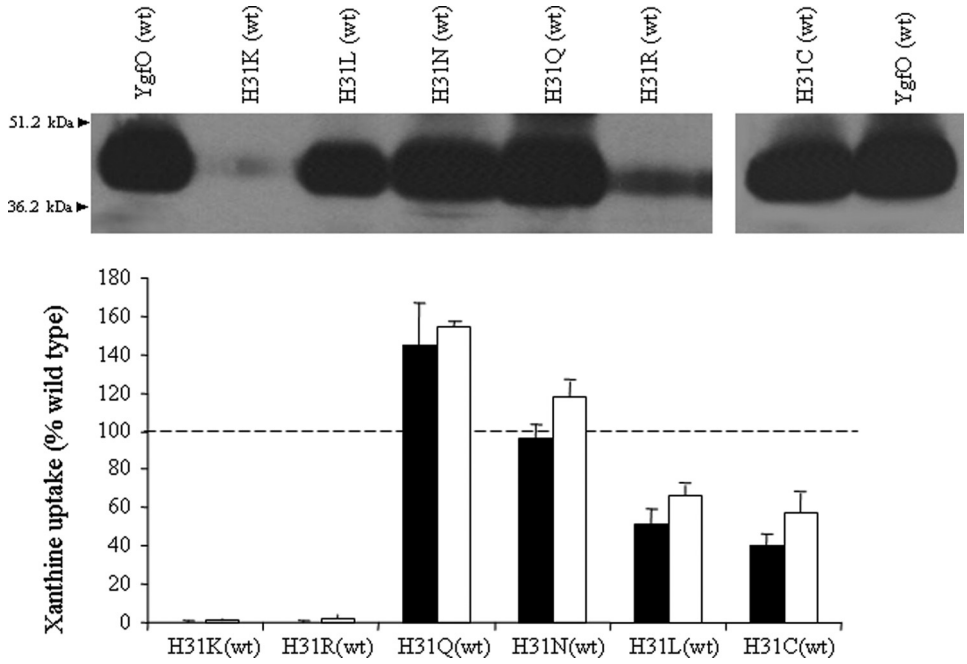

FIGURE 7. **Expression and xanthine uptake activities of site-directed mutants at position 31 (TM1).** *E. coli* T184 harboring pT7-5/*ygfO*(wild-type-BAD) with given mutations were grown, induced, and subjected to immunoblot analysis of membrane fractions (*upper panel*) or assayed for transport of [^{3}H]xanthine (1 μM, 25 °C) (*lower panel*) exactly as described in the legends for Figs. 3 and 4. *Open* and *closed histogram bars* represent the initial rate and steady state values, respectively.

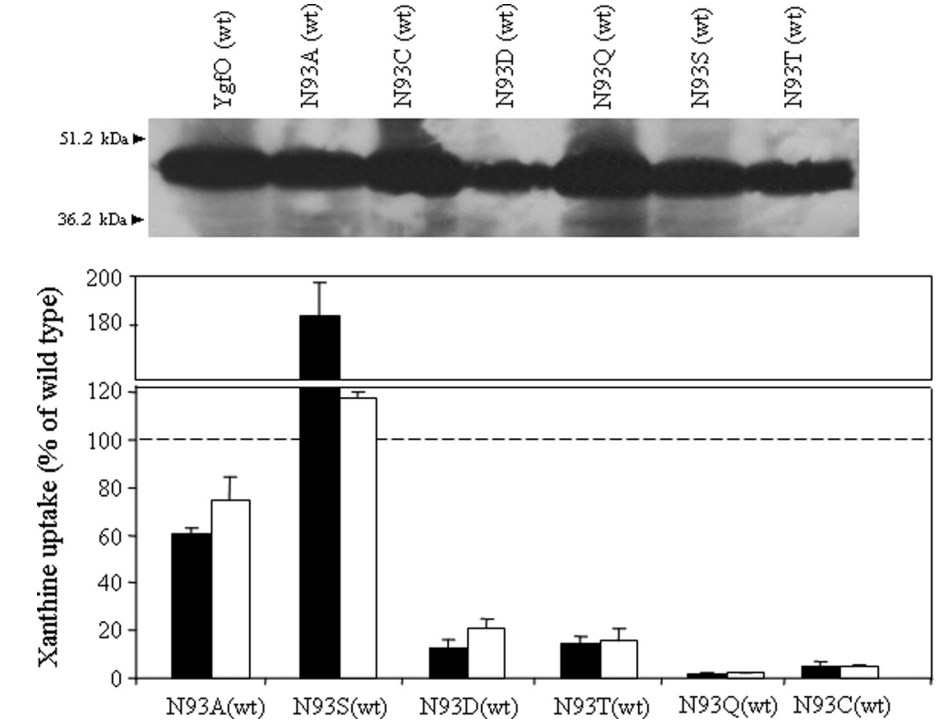

FIGURE 8. **Expression and xanthine uptake activities of site-directed mutants at position 93 (TM3).** *E. coli* T184 harboring pT7-5/*ygfO*(wild-type-BAD) with given mutations were grown, induced, and assayed exactly as described in the legend for Fig. 7.

inhibitory effect was evident in the presence of 1 mM xanthine (data not shown). On the other hand, activity of Q23C or K249C, which was about 50% of C-less initially (Fig. 3*A*), is enhanced in the presence of NEM almost 2-fold (Fig. 9), *i.e.* it is restored to C-less YgfO levels. The activity of the remaining 14 mutants is essentially unaltered in the presence of NEM (<1.2-fold enhancement or inhibition).

Site-directed Mutagenesis of Gln-258—The position of the low activity (Fig. 3) and NEM-sensitive mutant Q258C (Fig. 9) was subjected to more extensive site-directed mutagenesis in the wild-type YgfO background. Replacement of Gln-258 with Asn or His results in high xanthine uptake activity comparable with that of wild type (Fig. 5 and data not shown), whereas replacement with Cys results in lower activity (40% of wild type). Kinetic analysis shows that Q258N(wt) and Q258H(wt) transport xanthine with a K_m and V_{max} approximating the wild type (Table 1*D*). On transport inhibition experiments, Q258H(wt) was found to follow essentially wild-type selectivity for purine ligands, and Q258N(wt) was found to follow wild-type selectivity but also to recognize uric acid and guanine (Table 2). No transport of [^{14}C]uric acid was detected with these mutants at 2 mM (data not shown).

DISCUSSION

We have studied the role of 21 highly polar and/or charged residues in *E. coli* YgfO, the major xanthine-specific bacterial homolog of the NAT family and found that 4 of them are important for the function of the YgfO permease in various aspects. In summary, His-31 (TM1) and Asn-93 (TM3) are crucial for affinity and/or specificity against purine analogues, whereas Glu-272 (TM8) and Asp-304 (TM9a) are irreplaceable for active xanthine transport. Taken together with our previous findings on the irreplaceable role of Gln-324 and Asn-325 in the NAT motif sequence (9) and on Asn-430 in TM12 being in the vicinity of the purine binding site (10), these data suggest that polar residues critical for the mechanism of YgfO cluster in TMs 1, 3, 8, 9a, and 12 and the NAT motif sequence (Fig. 1).

The two irreplaceable residues of YgfO delineated here, Glu-272 and Asp-304, are highly conserved in the NAT family. Glu-272, at the cytoplasmic side of putative TM8, shows a nearly invariable conservation among the functionally known mem-

TABLE 2

Specificity profile of YgfO mutants at positions His-31, Asn-93, and Gln-258

Values shown express the percentage of [^{3}H]xanthine (1 μM) uptake rate in the presence of 1000-fold excess (1 mM) of unlabeled competitors. The uptake value obtained in the absence of competitor was taken as 100%. Values represent the means of at least three determinations ± S.D. (always <20%). Most significant differences from the wild-type profile are highlighted in bold. All mutants as well as the wild-type version used in these experiments contained a C-terminal BAD. All mutants assayed, including H31C, were in the wild-type YgfO background (WT). The purine bases or analogues used as potential competitors are: hypoxanthine (HX); uric acid; adenine; guanine; uracil; 1-methylxanthine (1-MX); 2-thioxanthine (2-SX); 3-methylxanthine (3-MX); 6-thioxanthine (6-SX); 7-methylxanthine (7-MX); 8-methylxanthine (8-MX); allopurinol; oxypurinol.

Competitor	WT	% [^{3}H]Xanthine uptake rate retained									
		His-31 mutants				Asn-93 mutants				Gln-258 mutants	
		H31N	H31Q	H31L	H31C	N93A	N93S	N93T	N93D	Q258N	Q258H
None	100	100	100	100	100	100	100	100	100	100	100
HX	99	88	99	89	88	112	88	104	85	67	78
Uric acid	96	**61**	**52**	99	98	**60**	**49**	115	73	**26**	94
Adenine	110	95	89	133	120	128	89	113	116	95	90
Guanine	89	68	**46**	91	102	67	65	65	80	**33**	67
Uracil	101	97	**48**	98	99	95	95	120	85	85	87
1-MX	45	44	39	**113**	**117**	43	38	**123**	77	42	48
2-SX	14	4	3	**91**	**91**	16	7	43	12	6	15
3-MX	28	19	16	**70**	**63**	41	16	49	38	39	44
6-SX	20	24	4	**123**	**102**	24	11	**84**	22	10	15
7-MX	100	76	**42**	162	84	**62**	**54**	121	**26**	116	124
8-MX	91	**33**	**25**	87	84	**9**	**9**	69	**25**	69	97
Allopurinol	101	91	98	80	84	110	84	161	132	113	147
Oxypurinol	30	5	4	**82**	**74**	2	16	13	1	14	23

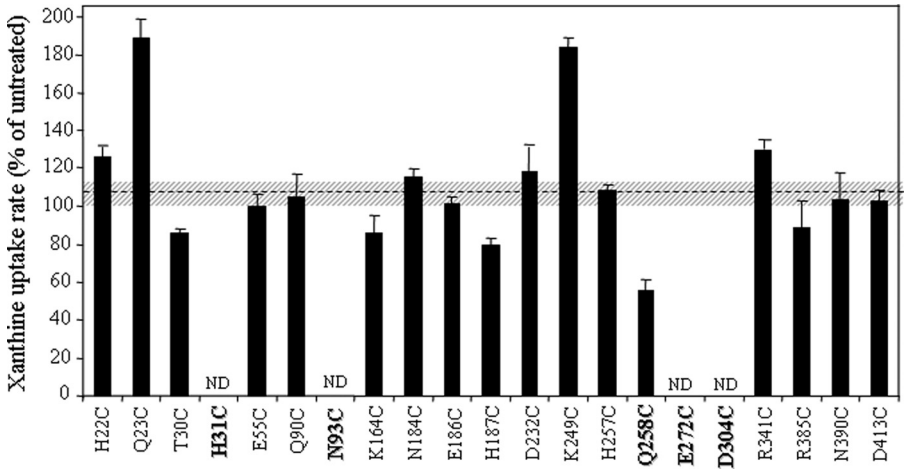

FIGURE 9. **Effect of NEM on the xanthine transport activity of single-Cys mutants.** *E. coli* T184 harboring pT7-5/*ygfO*(C-less-BAD) with given mutations were grown, induced, and assayed for transport of [^{3}H]xanthine (1 μM, 25 °C). Cells had been preincubated for 10 min at 25 °C in the absence or presence of 2 mM NEM. Transport assays were performed in the presence of 20 mM potassium ascorbate and 0.2 mM phenazine methosulfate. Rates are presented as percentages of the rate measured in the absence of NEM with standard deviations from three independent determinations shown. Average and standard deviation values of C-less control are also shown as a *broken line* and *gray horizontal bars*, respectively. Values were not determined (*ND*) for mutants H31C, N93C, E272C, and D304C, which display very low or negligible uptake rates.

bers, whereas the position of Asp-304, in the ambiguous, putative transmembrane TM9a, is occupied by Asp, Asn, or Glu (Fig. 2). The corresponding residues of the major fungal homolog UapA from *A. nidulans*, namely Glu-356 and Asp-388, were also delineated as absolutely essential for xanthine/uric-acid uptake in a recent random mutagenesis study (7). It is important to note that Asp-304 of YgfO is at an amphipathic, putative transmembrane segment (TM9a) preceding the conserved NAT signature motif (residues 323–333). We have previously shown that the motif region contains two functionally irreplaceable residues, Gln-324, which is essential for high affinity binding and uptake, and Asn-325, which also interferes with substrate binding,[3] as well as residues important for substrate analogue selectivity that fall on the NEM-sensitive α-helical face of TM9b (Fig. 1) (9). In addition, functional evidence suggests that this region is close in the tertiary structure to the middle of TM12, which contains Asn-430, another putative substrate-binding residue (10). It is conceivable, therefore, that Asp-304 (TM9a), 20 residues upstream of the NAT motif region, is situated close to but not at the purine binding site of YgfO and may be essential for the conformational changes following binding and/or coupling purine with proton translocation. Similar assumptions could be made for Glu-272 (TM8), because the middle of TM8 (His-257) appears to be in proximity with TM12 and the NAT motif region, based on cadmium sensitivity assays with single- and double-Cys mutants.[7] In this vein, site-directed alkylation shows that D304C reacts slowly with NEM in right-side-out membrane vesicles, and reactivity is enhanced in the presence of xanthine, implying that (*a*) replacement of Asp-304 is compatible with high affinity substrate binding and (*b*) Asp304 is highly sensitive to the conformational movements associated with the permease turnover.[7] Further experiments to elucidate the role of Asp-304 and Glu-272 in more detail are under way in our laboratory.

Residue His-31, at the middle of TM1, is almost completely conserved in the NAT family (2) and is preceded by a polar residue, which is Thr-30 in YgfO and Gln in all other NAT transporters (Fig. 2). From our results, it is apparent that His-31 is replaceable for YgfO function, but the presence of a hydrogen-bonding uncharged residue at this position is essential for high affinity binding and transport; high capacity and affinity

[7] E. Karena and S. Frillingos, unpublished observations.

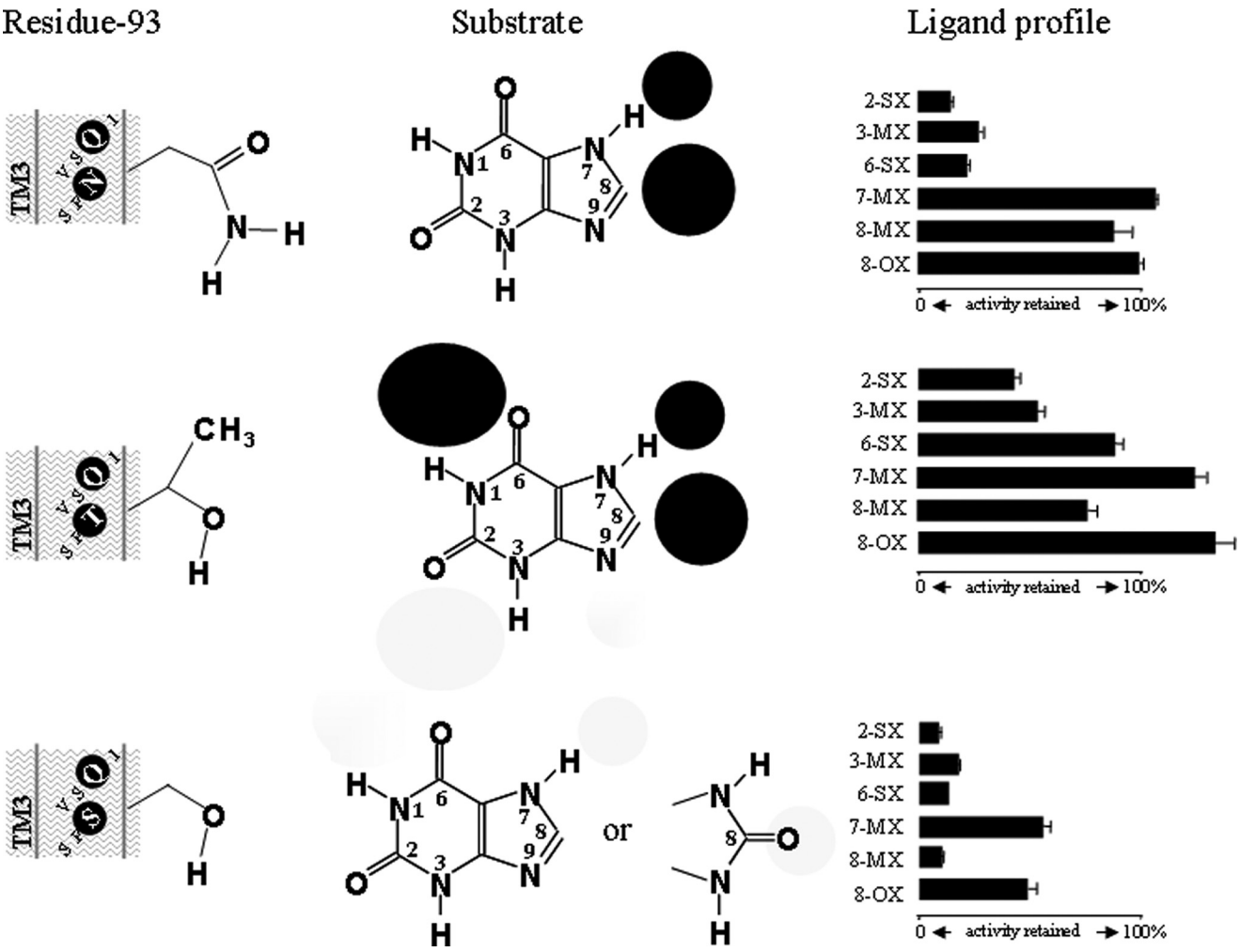

FIGURE 10. **Substrate recognition properties of mutants replacing Asn93.** Shown is the side chain of residue 93 for wild type (*top*), N93T (*middle*), and N93S (*bottom*) with respect to their purine substrate usage and constraints and characteristic changes in the specificity profile (data from Table 2). *Shaded circular areas* denote numbered positions of the purine ring where a bulkier substitution abolishes recognition (≥70% xanthine uptake activity retained in the presence of the putative competitor) (*black*) or results in poor recognition (45–60% activity retained) (*gray*). The purine bases or analogues shown are: 2-thioxanthine (*2-SX*); 3-methylxanthine (*3-MX*); 6-thioxanthine (*6-SX*); 7-methylxanthine (*7-MX*); 8-methylxanthine (*8-MX*); uric acid (8-oxy-xanthine) (*8-OX*).

for xanthine uptake is retained upon replacement with Asn or Gln, whereas a hydrophobic (Leu) or low polarity (Cys) replacement impairs affinity for substrate, and introduction of a positive charge through side-specific mutagenesis (Lys, Arg) or alkylation with (2-aminoethyl)methanethiosulfonate[7] abolishes expression and/or activity. Interestingly, the same contention has been reached on the role of the corresponding residue, His-51, in the mammalian, non-purine-transporting homolog hSVCT1 (21), whereas hydrogen bonding of His-86 at the corresponding consensus position of the fungal UapA has been suggested as crucial for proper folding and targeting to the plasma membrane (5). On the other hand, we find that introduction of a more flexible hydrogen-bonding side chain (Gln) in lieu of His-31 leads to a novel specificity profile with broader recognition of purine bases and analogues (Table 2). A specificity change leading to a novel property (recognition of the oxidized form of L-ascorbic acid) has also been reported with mutant H51Q in hSVCT1 (21), and the corresponding H86Q mutant has not been made in UapA (5). Taken together, evidence from the mutagenesis studies of His-31 in mammalian (21), fungal (5), and bacterial (this study) NAT systems points to a conserved hydrogen bonding role of this residue, which is crucial for either the overall structural folding or the constitution of a proper affinity and specificity binding site or for both. Finally, His-31 is part of a conserved QH sequence motif (Fig. 2), and the preceding Gln residue has been indicated as important for transport catalysis in both hSVCT1 (21) and UapA (5). We found no evidence for such a role from the mutagenesis of the corresponding residue of YgfO (Thr-30) in this study.

Residue Asn-93, at the middle of TM3, is not conserved as an amidic side chain in the other members of the NAT family, but the nucleobase-transporting members retain a hydrogen-bonding Thr or Ser, and the mammalian SVCTs have an Ala at this position. Replacement of Asn-93 with a small hydrophobic (Ala) or hydrophilic (Ser) residue yields very high xanthine uptake activity, which is comparable (Ala) or higher (Ser) than wild type, but changes the purine selectivity of YgfO by relaxing constraints for binding at the imidazole moiety of substrate. Thus, these mutants are very efficient in recognizing 8-methylxanthine and, to a lesser extent, 7-methylxanthine and uric acid (8-oxy-xanthine), and they even transport [^{14}C]uric acid with low capacity or affinity, properties that are not pertinent to

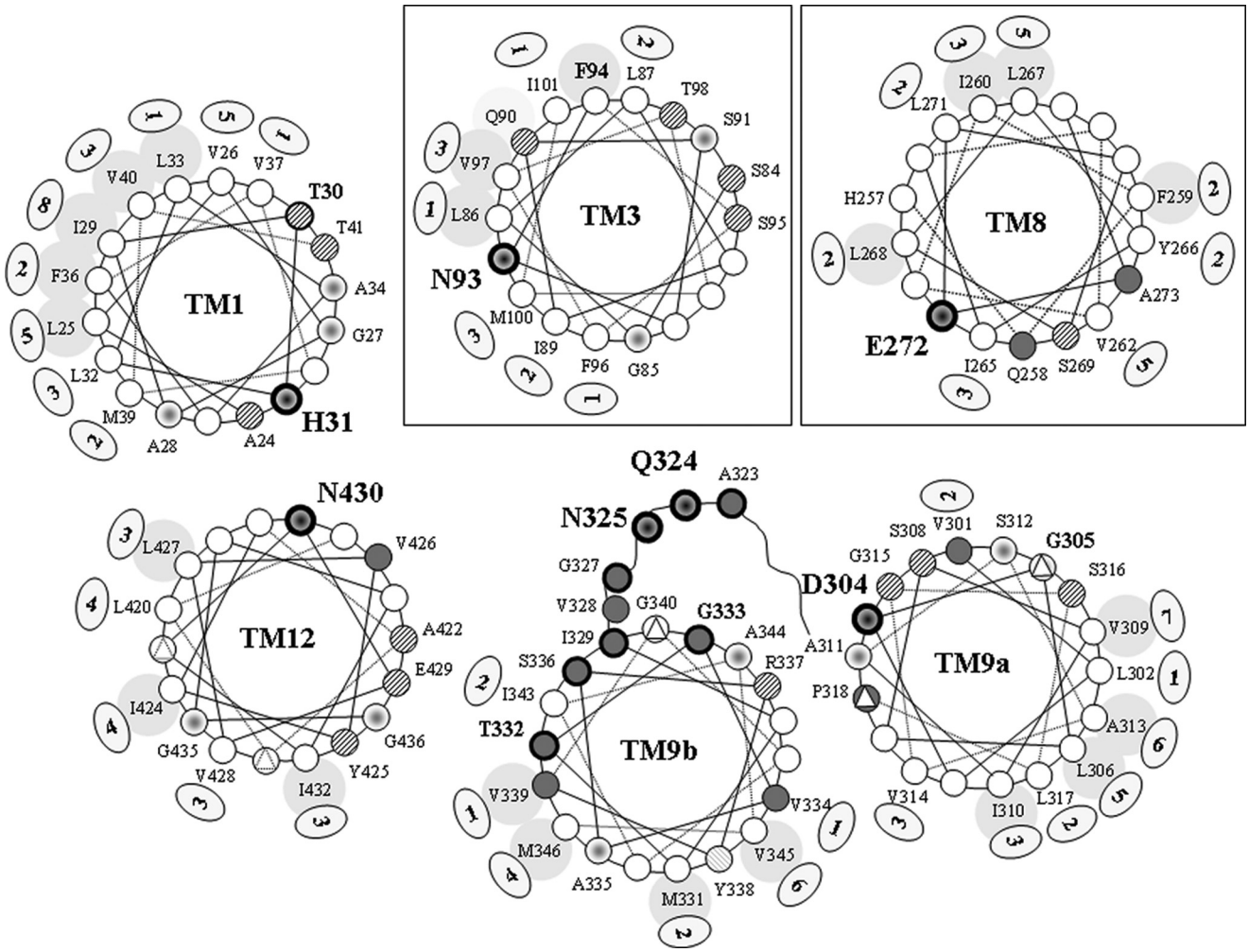

FIGURE 11. **Hypothetical arrangement of TM1, TM3, TM8, TM9a, TM9b, and TM12 in YgfO permease viewed from the cytoplasmic surface.** Segments of the YgfO sequence are shown as *helical wheel plots* of residues 24–41 (TM1), 84–101 (TM3), 257–274 (TM8), 301–318 (TM9a), 329–346 (TM9b), and 419–436 (TM12). The placement of TM3 and TM8 (*insets*) is more tentative, as analyzed under "Discussion". The polar residues delineated as important from our studies are *enlarged* and *bolded* and shown as targets. Sites of NEM-sensitive single-Cys mutants in TM8, TM9a,[8] the NAT motif sequence (9), TM9b (9), and TM12 (10) are shown with a *dark background*, and highly sensitive sites ($IC_{50} \leq 30\ \mu M$) are shown with *bolder peripheries*. Sites where mutants impair folding or stability in the membrane are indicated with a *triangle*. The sites of Pro-421 and Pro-431 in TM12 where mutants do not impair expression or activity (10) are indicated with a *broken line triangle*. The NAT motif sequence (9) is shown as a putative reentry loop with Gln-324 and Asn-325 pointing toward the solvent-accessible internal cavity. Residues conserved either *per se* or with respect to their side-chain character in the known members of the family are shown *enlarged* (see also Fig. 2). Sites conserving a hydrophobic side chain in the known members are indicated by a *larger light gray area* facing outside the helix. Sites conserving hydrophobic residues in the 67 closest sequence homologs of YgfO (sequence identity $\geq$ 43%) are indicated by an additional *small oval* at the outside of the helix with a *number* denoting the number of different amino acid replacements found at each position. Sites conserving a hydrophilic residue or a small side chain in the cohort of the 67 closest homologs are shown as *hatched circles* or *targets*, respectively. The site of Thr-30, almost invariably conserving a Gln or Thr throughout the family, is indicated with a *bolder periphery*.

wild-type YgfO. On the other hand, replacement with a polar residue of comparable volume (Thr) yields low affinity, possibly due to loss of a bi-dentate hydrogen-bonding interaction of Asn-93 (Fig. 10). Introduction of a more bulky carboxyl amide (Gln) or a sulfur-containing, less polar side chain (Cys) in lieu of Asn-93 leads to inactivation, suggesting that both steric and polarity constraints at position 93 are important for function. Finally, the low activity observed with mutant N93D suggests that introduction of a negative charge at this position may also be unfavorable for function. It is interesting to note that replacement of Asn-93 with amino acids encountered at the corresponding residue position of the other NAT transporters (Fig. 2) yields YgfO versions with modified specificity (Fig. 10). Replacement with Ser, in particular, which is conserved in the uric-acid/xanthine transporters Xut1, UapA, UapC, AfUapA, and Lpe1, yields efficient recognition of analogues at the imidazole moiety of substrate, mimicking in part the fungal or plant members (Fig. 10).

Because a high-resolution x-ray structure of a NAT prototype is not available to date (22), to understand the putative spatial association of the important residues delineated herein with the ones reported previously (9, 10) we performed a detailed sequence analysis of NAT homologs, and in conjunction with available biochemical data and the assumption that the conserved highly polar/charged residues (18) should face away from the lipid, we deduced a naive helix packing model for YgfO (Fig. 11). In this model, the NAT motif sequence is shown as a putative loop facing toward the central hydrophilic cavity, based on *in silico* analysis (4) and evidence that 10 consecutive residues of this sequence are highly sensitive to site-directed

alkylation (9) and accessible to solvent,[6] with at least one of them, Gln-324 (9) or its counterpart in the fungal UapA (4), implicated directly with substrate binding. Placement of the NEM-sensitive face of helix TM9a close to the stripe of small and/or hydrophilic residues of TM12 is supported by functional evidence for interaction between TM12 and the NAT motif region in both a bacterial (10) and a fungal (7) transporter. As shown with other transporters (23–25), such NEM-sensitive faces are expected to be conformationally active or to line the substrate translocation pathway and be critical for the mechanism. Placement of TM8 close to both the NAT motif and TM12 is supported by cadmium-sensitivity assays.[7] Placement of TM1 close to TM12 as well as to the NAT motif region has been proposed from extensive second-site suppressor analysis in the fungal UapA (7). Finally, although placement of TM3 is tentative, an interaction between the fungal TM3 (M151) and TM1 (H86) is indicated from a second-site suppressor study.[8]

Of the important residues described, His-31 and Asp-304 fall in polar/small side-chain and/or alkylation-sensitive faces of amphipathic α-helical segments (Fig. 11) with extensive lipid-facing stripes of residues on the other side. A similar, but less prominent, effect is seen with Asn-430 in TM12 and the NEM-sensitive face of TM9b. On the other hand, Asn-93 (TM3) is on the opposite side of a polar face of the helical wheel, and Glu-272 (TM8) is not connected to a contiguous polar stripe, suggesting that TM3 and TM8 could be discontinuous helices or tilted with respect to the plane of the membrane and/or participate in multiple hydrophilic contacts with other helices. With respect to TM8, Cys-scanning analysis[9] shows that a broader face of positions of NEM-sensitive and/or low activity mutants is formed at the cytoplasmic side, including Ser-269, Glu-272, Ala-273, Gly-275, and Asp-276. Thus, TM8 might extend by one additional helical turn (Fig. 1), introducing Asp-276 as another putative intramembrane charged residue, one turn above Glu-272. Mutagenesis of Asp-276 indicates that a carboxylic group at this position may also be important for function.[9] In any event, it is clear that all of the helices in Fig. 11 contain important residue sites, including Gln-324 (9) and Asn-430 (10), which interfere with substrate binding. It would be interesting to test whether the newly identified determinants of affinity and/or specificity, His-31 and Asn-93, are also proximal to the binding site or act by indirect, long-range effects. Site-directed sulfhydryl alkylation cannot be used as a tool to this end, because the corresponding Cys replacement mutants are either inactive or grossly impaired for substrate affinity (Fig. 3; Tables 1 and 2). For example, we found that H31C is alkylatable with NEM *in situ* and H31C(wt) is sensitive to inactivation by NEM, but no protective or other effect is evident in the presence of xanthine,[7] most probably because of the inability of these mutants to bind the xanthine substrate with high affinity.

In conclusion, we have provided evidence for four new important players in the mechanism of the YgfO permease and shown that their role is probably conserved in the NAT/NCS2 family of transporters. Ongoing work on the bacterial (YgfO) and fungal (UapA) NAT prototypes, in conjunction with potential future structural studies (22), is expected to shed light on the mechanism and evolution of purine substrate recognition and selectivity in this important, evolutionarily ubiquitous family of nucleobase-ascorbate transporters.

Acknowledgments—We thank H. Ronald Kaback and George Diallinas for helpful discussions and Ekaterini Georgopoulou for help with site-directed alkylation experiments.

[8] A. Pantazopoulou and G. Diallinas, personal communication.
[9] G. Mermelekas, A. Kallis, and S. Frillingos, manuscript in preparation.

REFERENCES

1. Tsukaguchi, H., Tokui, T., Mackenzie, B., Berger, U. V., Chen, X. Z., Wang, Y., Brubaker, R. F., and Hediger, M. A. (1999) *Nature* **399,** 70–75
2. Gournas, C., Papageorgiou, I., and Diallinas, G. (2008) *Mol. Biosyst.* **4,** 404–416
3. Diallinas, G., Valdez, J., Sophianopoulou, V., Rosa, A., and Scazzocchio, C. (1998) *EMBO J.* **17,** 3827–3837
4. Koukaki, M., Vlanti, A., Goudela, S., Pantazopoulou, A., Gioule, H., Tournaviti, S., and Diallinas, G. (2005) *J. Mol. Biol.* **350,** 499–513
5. Pantazopoulou, A., and Diallinas, G. (2006) *Mol. Membr. Biol.* **23,** 337–348
6. Vlanti, A., Amillis, S., Koukaki, M., and Diallinas, G. (2006) *J. Mol. Biol.* **357,** 808–819
7. Papageorgiou, I., Gournas, C., Vlanti, A., Amillis, S., Pantazopoulou, A., and Diallinas, G. (2008) *J. Mol. Biol.* **382,** 1121–1135
8. Karatza, P., and Frillingos, S. (2005) *Mol. Membr. Biol.* **22,** 251–261
9. Karatza, P., Panos, P., Georgopoulou, E., and Frillingos, S. (2006) *J. Biol. Chem.* **281,** 39881–39890
10. Papakostas, K., Georgopoulou, E., and Frillingos, S. (2008) *J. Biol. Chem.* **283,** 13666–13678
11. Abramson, J., Smirnova, I., Kasho, V., Verner, G., Kaback, H. R., and Iwata, S. (2003) *Science* **301,** 610–615
12. Boudker, O., Ryan, R. M., Yernool, D., Shimamoto, K., and Gouaux, E. (2007) *Nature* **445,** 387–393
13. Faham, S., Watanabe, A., Besserer, G. M., Cascio, D., Specht, A., Hirayama, B. A., Wright, E. M., and Abramson, J. (2008) *Science* **321,** 810–814
14. Weyand, S., Shimamura, T., Yajima, S., Suzuki, S., Mizra, O., Krusong, K., Carpenter, E. P., Rutherford, N. G., Hadden, J. M., O'Reilly, J., Ma, P., Saidijam, J., Patching, S. G., Hope, R. J., Norbertczak, H. T., Roach, P. C., Iwata, S., Henderson, P. J., and Cameron, A. D. (2008) *Science* **322,** 709–713
15. Inoue, H., Nojima, H., and Okayama, H. (1990) *Gene* **96,** 23–28
16. Teather, R. M., Bramhill, J., Riede, I., Wright, J. K., Fürst, M., Aichele, G., Wilhelm, V., and Overath, P. (1980) *Eur. J. Biochem.* **108,** 223–231
17. Granseth, E., Daley, D. O., Rapp, M., Mélen, K., and von Heijne, G. (2005) *J. Mol. Biol.* **352,** 489–494
18. Baldwin, J. M. (1993) *EMBO J.* **12,** 1693–1703
19. Frillingos, S., and Kaback, H. R. (1996) *Biochemistry* **35,** 13363–13367
20. Frillingos, S., Sahin-Tóth, M., Lengeler, J. W., and Kaback, H. R. (1995) *Biochemistry* **34,** 9368–9373
21. Varma, S., Campbell, C. E., and Kuo, S. M. (2008) *Biochemistry* **47,** 2952–2960
22. Stroud, R. M., Choe, S., Holton, J., Kaback, H. R., Kwiatkowski, W., Minor, D. L., Riek, R., Sali, A., Stahlberg, H., and Harries, W. (2009) *J. Struct. Funct. Genomics* **10,** 193–208
23. Frillingos, S., Sahin-Tóth, M., Wu, J., and Kaback, H. R. (1998) *FASEB J.* **12,** 1281–1299
24. Tamura, N., Konishi, S., Iwaki, S., Kimura-Someya, T., Nada, S., and Yamaguchi, A. (2001) *J. Biol. Chem.* **276,** 20330–20339
25. Tavoulari, S., and Frillingos, S. (2008) *J. Mol. Biol.* **376,** 681–693